Current Applied Physics 14 (2014) 127–131

Contents lists available at ScienceDirect

Current Applied Physics

journal homepage: www.elsevier.com/locate/cap

Silicon nanoparticle size-dependent open circuit voltage in an organic–inorganic hybrid solar cell

Seongbeom Kim [a,*], Jae Hee Lee [b], Mark T. Swihart [c], Jeong-Chul Lee [b,*], Jin Young Kim [a,*]

[a] Interdisciplinary School of Green Energy, Ulsan National Institute of Science and Technology (UNIST), Ulsan 689-798, Republic of Korea
[b] KIER UNIST Advanced Center for Energy, Korea Institute of Energy Research, Ulsan 689-798, Republic of Korea
[c] Department of Chemical and Biological Engineering, The University at Buffalo (SUNY), Buffalo, NY 14260-4200, United States

ARTICLE INFO

Article history:
Received 10 June 2013
Received in revised form
16 September 2013
Accepted 7 October 2013
Available online 30 October 2013

Keywords:
Silicon nanoparticle
Silicon nanocrystal
Hybrid solar cell
Organic inorganic solar cell

ABSTRACT

We have incorporated silicon nanoparticles (Si-nps) into organic–inorganic hybrid solar cells in place of the chalcogenide nanocrystals that are commonly employed in such devices. Poly(3,4-ethylenedioxy-thiophene):poly(styrene sulfonate) (PEDOT:PSS) and phenyl-C_{61}-butyric acid methyl ester (PCBM) were employed as hole and electron transport layers, respectively. We used transmission electron microscopy, Raman spectroscopy, and ultraviolet–visible spectroscopy to fully characterize the Si-nps and relate their characteristics to the performance of the hybrid solar cells. We show that the open circuit voltage (V_{OC}) was largely dependent on the size and amorphous volume fraction of Si-nps. Our findings imply that the amorphous phase and small size of Si-nps produce band gap widening that increases the V_{OC} when coupled with PCBM as acceptor. The maximum V_{OC} was up to 0.634 V in a hybrid device with 5.7 nm Si-nps.

1. Introduction

Numerous attempts have been made to harvest solar energy using a combination of inorganic nano-structured materials and polymers [1–4] because inorganic nano-structured materials have superior electronic properties to polymers while retaining the high absorption of polymers. Furthermore, these hybrid architectures can provide large interfacial area where charge separation occurs, along with directed pathways for rapid carrier conduction to a set of carrier-selective electrodes [3]. Adoption of simple and easy techniques for thin film fabrication from liquid solutions or dispersions makes hybrid photovoltaic devices attractive as well. Most of these organic–inorganic hybrid solar cells use chalcogenide nanocrystals as a counterpart of polymer materials because the synthesis procedures for the chalcogenides are well established [5] and their band gap can be controlled by reducing the size of nanocrystals due to quantum confinement effects. However, from a long-term perspective, use of materials that generate the environmental and toxicity concerns associated with heavy-metal chalcogenides is problematic. Thus, replacing these nanocrystals with inorganic nanoparticles of non-toxic, earth-abundant elements remains of great interest.

Several reports have been published about hybrid solar cells which use silicon nanoparticles (Si-nps) [6–9], taking advantage of the development of macro-scale methods of producing Si-nps [10,11]. Silicon is the most well-known semiconductor material and is both earth abundant and non-toxic in elemental form. Si-nps have been used as a counterpart of polymer materials, for example, as an electron acceptor [6], or an electron donor [7] according to the energy level of polymer materials. We have previously shown that addition of etched Si-nps increased the performance of polymer bulk-heterojunction solar cells [9]. The relationship between the size of Si-nps and performance of hybrid solar cells has been reported for one device configuration [12]. However, the specific Si-np properties that are required to achieve efficient hybrid solar cells remain uncertain.

Here we have produced Si-nps by laser pyrolysis, and characterized them using transmission electron microscopy (TEM), Raman spectroscopy and ultraviolet–visible absorbance spectroscopy (UV–Vis) to relate Si-np physical properties (e.g. size and crystallinity) to hybrid solar cell performance. We used poly(3,4-ethylenedioxy-thiophene):poly(styrene sulfonate) (PEDOT:PSS) and phenyl-C_{61}-butyric acid methyl ester (PCBM) as hole and electron transport layers, respectively. The performance of hybrid solar cells was measured using current–voltage sweeps under illumination from a solar simulator. We measured the changes in

* Corresponding authors.
E-mail addresses: exebac@gmail.com (S. Kim), jclee@kier.re.kr (J.-C. Lee), jykim@unist.ac.kr (J.Y. Kim).

1567-1739/$ – see front matter © 2013 Elsevier B.V. All rights reserved.
http://dx.doi.org/10.1016/j.cap.2013.10.006

open circuit voltage (V_{OC}) resulting from changes in the size and degree of crystallinity.

2. Experimental details

2.1. Synthesis of Si-nps via laser pyrolysis of SiH_4

Si-nps were synthesized by the laser pyrolysis method [10], because laser pyrolysis of SiH_4 can produce relatively large quantities of free-standing Si-nps. The reactor was designed such that the three axes of laser beam pathway, gas flow, and view port line-of-sight crossed at a single point, as illustrated in Fig. 1. The Si-np synthesis begins with fast nucleation of solid particles from the reactive species generated by dissociation of SiH_4 molecules following their absorption of the focused laser beam (10.6 μm wavelength). The Si-nps grow by surface reaction with additional silane and silane decomposition products, and by collision and coalescence with one another. Very rapid initiation of nucleation, using laser heating, and quenching of particle growth by mixing with the surrounding gas after leaving the laser beam allow production of very small particles. Typically ~300 mg/h of Si-nps could be collected when the laser pyrolysis was driven by a 60 W maximum power CO_2 laser. This production yield corresponds to ~20% gas-to-solid conversion efficiency.

As-produced Si-nps were collected on a membrane filter within a tightly sealed container and transferred to a N_2-filled glove box to protect them from exposure to the air. For spin-coating of Si-np films, the Si-nps were dispersed into benzonitrile. We selected benzonitrile based on reports of producing stable colloidal inks of germanium nanoparticles [13] and silicon–germanium nanoparticles [14] using benzonitrile. In addition, it does not damage the underlying PEDOT:PSS layer during the spin coating process. Typically, 100 mg Si-nps was dispersed into 10 ml of benzonitrile, then several hours of mild sonication were applied to break up agglomerated Si-nps. Precipitated large Si-np aggregates were separated by centrifugation and, finally, a stable Si-np dispersion was achieved. The Si-nps dispersion did not show any signs of precipitates over a period of at least two months.

2.2. Device fabrication

The fabrication of devices began with pre-cleaning of ITO-coated glass substrates using deionized water, acetone and isopropyl alcohol, sequentially. After UV-ozone treatment for about 10 min, PEDOT:PSS (Baytron P VPAI4083) was spin-coated onto the pre-cleaned ITO glass substrates and then the substrates were baked at 120 °C for 10 min to remove residual solvent. Spin coating of the Si-np dispersion and then PCBM (dissolved into dichlorobenzene, 1 wt%) followed, with baking at each step. The fabrication procedure was completed by deposition of aluminum electrodes using thermal evaporation.

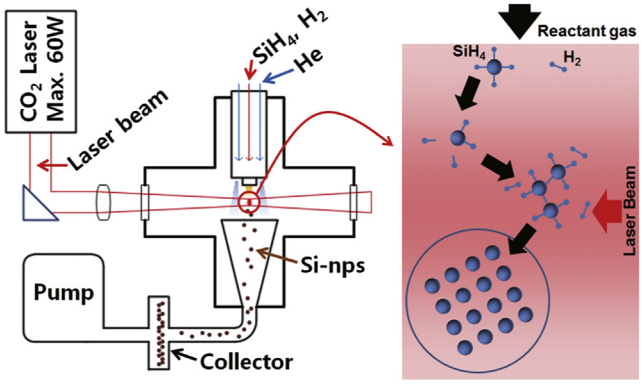

Fig. 1. A schematic of the reactor for producing Si-nps by laser pyrolysis of SiH_4. The laser beam pathway, gas flow direction and view port line of sight (perpendicular to the surface of this paper) are mutually perpendicular. The center of reaction zone is zoomed in to schematically illustrate the processes of dissociation of SiH_4 and growth of Si-nps.

3. Results and discussion

3.1. Characterization of Si-nps

In the growth process of Si-nps during laser pyrolysis, the addition of hydrogen gas plays an important role in determining the properties of final products. Hydrogen gas addition hinders Si-np growth both by diluting the silane precursor and by shifting the reaction equilibrium for silane decomposition (to silicon and hydrogen) back toward silane. Therefore, the size of Si-nps tends to decrease with increasing hydrogen flow rate [10]. The gas flow rates were fixed to 25 standard cubic centimeters per minute (sccm) of SiH_4 gases as the H_2 flow was varied from 50 to 100 sccm. The working pressure and the laser power were set to 400 mTorr and 57 W, respectively. Assuming that the Si-nps are quasi-spherical, we can measure their size from TEM images. The TEM images in Fig. 2 show that the average size of Si-nps was reduced when the hydrogen gas flow rate increased from 50 to 100 sccm. 50 individual Si-nps in TEM images were measured for each 3 batch of Si-nps. The average sizes of Si-nps were 10.8, 9.8 and 5.7 nm for 50, 80 and 100 sccm hydrogen gas flow, respectively. Also, the width of the size distribution decreased as the hydrogen gas flow rate increased, implying that the random rapid growth of Si-nps was interrupted by extra hydrogen gases. The standard deviations of the Si-nps size were 3.4, 2.5 and 0.9 nm for 50, 80 and 100 sccm hydrogen gas flow rate condition, respectively. High resolution TEM images (Fig. 2(b), (d) and (f)) clearly show that the two phases of silicon, amorphous and crystalline, exist together. For the smaller Si-nps, volume fraction of amorphous silicon within Si-nps is larger than for the larger Si-nps. Thus, the hydrogen gases not only reduce the size of Si-nps but also increase the amorphous silicon phase fraction within Si-nps. This is supported by Raman spectroscopy measurement of each sample as shown in Fig. 3(a). It is well known that the crystalline silicon shows sharp peak centered at 520 cm^{-1}, and amorphous silicon shows broad diffused spectral response around 480 cm^{-1} because of various bond angles, strength and energy along with an intermediate component peak at around 500 cm^{-1} which is associated with bond dilation at grain boundaries [15]. In the case of 10.8 nm Si-nps, the Raman spectroscopy results exhibited sharp peak at around 520 cm^{-1} with a small shoulder signal around 480 cm^{-1}. This indicates that the crystalline silicon is dominant in 10.8 nm Si-nps. A clear peak is also shown in 9.8 nm Si-nps at around 520 cm^{-1} with relatively increased signals at around 480 cm^{-1} compared with the 10.8 nm Si-nps. However, the sharp peak at around 520 cm^{-1} is reduced significantly in 5.7 nm Si-nps while the broad signal of amorphous silicon become dominant. The volume fraction of each component obtained by fitted the Raman spectra is summarized in Fig. 3(b), the volume fraction of amorphous silicon [16] determined in this way was 36.8%, 45.0% and 78.0% for 10.8, 9.8 and 5.7 nm Si-nps, respectively, implying that the amorphous phase fraction increased as hydrogen gas flow rate increased during the synthesis process. In terms of grain boundaries, the volume fraction of grain boundaries was 12.8, 15.6, and 7.7% for 10.8, 9.8 and 5.7 nm Si-nps, respectively. Fig. 3(c) presents UV–Vis absorption spectra from each Si-nps sample dispersed in benzonitrile. The 10.8 nm Si-nps dispersion absorbs light up to 1.1 eV which corresponds to the band gap of bulk silicon.